This item is the archived peer-reviewed author-version of:

Tunable electronic and magnetic properties of graphene/carbon-nitride van der Waals heterostructures

Journal Pre-proofs

Full Length Article

Tunable electronic and magnetic properties of graphene/carbon-nitride van der Waals heterostructures

A. Bafekry, B. Akgenc, S. Farjami Shayesteh, B. Mortazavi

Please cite this article as: A. Bafekry, B. Akgenc, S.F. Shayesteh, B. Mortazavi, Tunable electronic and magnetic properties of graphene/carbon-nitride van der Waals heterostructures, *Applied Surface Science* (2019), doi: https://doi.org/10.1016/j.apsusc.2019.144450

Tunable electronic and magnetic properties of graphene/carbon-nitride van der Waals heterostructures

A. Bafekry[a,b,*], B. Akgenc[c], S. Farjami Shayesteh[a], B. Mortazavi[d]

a Department of Physics, University of Guilan, 41335-1914 Rasht, Iran
b Department of Physics, University of Antwerp, Groenenborgerlaan 171, B-2020 Antwerp, Belgium
c Department of Physics, Kirklareli University, Kirklareli, Turkey
d Institute of Continuum Mechanics, Leibniz Universitt Hannover, Appelstrae 11, 30157 Hannover, Germany

Abstract

In this paper, we explore the electronic properties of C_3N, C_3N_4 and C_4N_3 and graphene (Gr) van der Waals heterostructures by conducting extensive first-principles calculations. The acquired results show that these heterostructures can show diverse electronic properties, such as the metal (Gr on C_3N), semiconductor with narrow band gap (Gr on C_3N_4) and ferromagnetic-metal (Gr on C_4N_3). We furthermore explored the effect of vacancies, atom substitution, topological, antisite and Stone-Wales defects on the structural and electronic properties of considered heterostructures. Our results show that the vacancy defects introduce localized states near the Fermi level and create a local magnetic moment. The Gr/C_3N heterostructures with the single and double vacancy defects exhibit a ferromagnetic-metal, while Stone-Wales defects show an indirect semiconductor with the band gap of 0.2 eV. The effects of adsorption and insertion of O, C, Be, Cr, Fe and Co atoms on the electronic properties of Gr/C_3N have been also elaborately studied. Our results highlight that the electronic and magnetic properties of garphene/carbon-nitride lateral heterostructures can be effectively modified by point defects and impurities.

Keywords: Density Functional Theory, Electronic properties, Graphene-based heterostructures, Defect, Atom impurity

1. Introduction

Tunability of electronic and magnetic properties is a hallmark of low dimensional systems, making them ideally suited for various applications. In recent years various approaches such as embedding of atoms, defect engineering, surface functionalization and application of electric fields have been investigated to modify the electronic and magnetic properties of two-dimensional (2D) materials. The discovery of graphene has spurred a surge in the study of 2D materials during the past decade. 2D materials have become a leading area of interest in the field of material science and engineering due to having unique combination of superlative on technological applications. [1, 2] The major drawback, which deal with graphene in many potential device applications, is its zero band gap. [3] The fabrication of laterally grown graphene-boron nitride hybrid structure is one of the approaches suggested for tuning the band gap. [4–6] Though the lattice parameters of graphene and 2D carbon nanotube are nearly equal, their electronic properties show semiconducting property intermediate between semi-metallic graphene and insulating h-BN nanosheets in the modeling of hybrid 2D ternary system (composed of B, C and N atoms). [7] The various layered binary composites BC_3, C_3N_4 as well as ternary composites BCN, BC_2N, BC_4N etc. have composed of mixing C, B and N atoms with different stoichiometries. [8–10] Recent efforts have focused on taking advantage of the individual properties of different 2D materials by fabricating heterostructures (HTS), which are vertical stacks of 2D layers of dissimilar materials held together by vdW forces. Gr/MoS_2 [11], Gr/h-BN [12–14], Gr/silicene [15–17] Gr/phosphorene [18, 19], C$_3$N4-MoS2 [20] heterojunctions [21, 22] with vdW HTS foces have been widely studied experimentally and theoretically. They preserve their intrinsic electronic properties and create outstanding advantageous electronic engineering. In addition the vertical stacking of magnetic metal phases with graphene can be potentially useful for promising graphene-based spintronic applications. [23]

Very recently, carbon-nitride 2D materials are gaining remarkable attentions due to their highly desirable properties for the practical applications in nanoelectronics, sensors, catalysis, thermal managements and many other advanced technologies. [24, 25] The thinnest layered 2D crystal (designated as C_2N-h2D crsytal) have been synthesized by Javeed et al. [26] and was found to semiconducting with 1.96 eV band gap stem from sp^2 hybridization. Due to its porous structure and light mass the recently synthesized triazine-based graphitic C_3N_4 sheet is a promising material as a hydrogen storage material [27]. Transition metal (TM) atoms embedded 2D graphitic C_3N_4 stacked graphene has experimentally synthesized. The charge-transfer analysis demonstrated that TM-C_3N_4 transfers electrons from the d-orbital to conduction band of graphene; making it n-doped in nature. [28] Based on hybrid density functional theory, g-C_4N_3 have showed semiconductor with a small band gap, sharp optical absorption peaks and high absoption intensity. [12] The
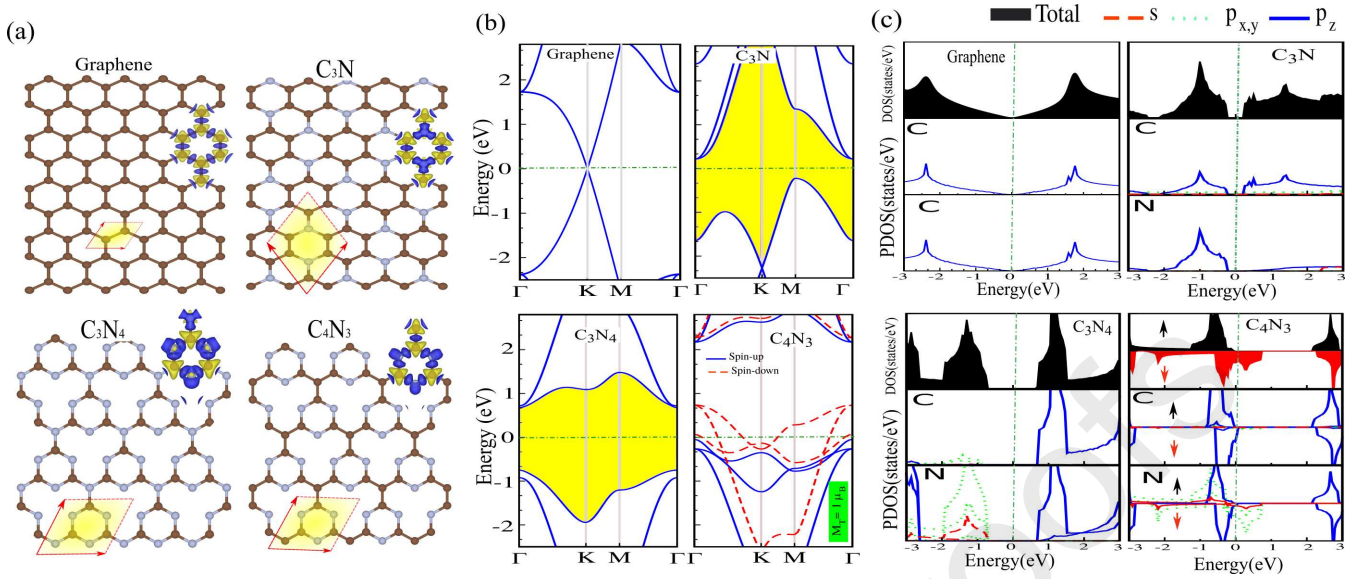
Figure 1: (a) Geometric atomic structures, (b) Electronic structure and (c) DOS and PDOS of graphene, C_3N, C_3N_4 and C_4N_3 monolayers. With the brown atoms representing C and the blue atoms representing N. The primitive unit cell indicated by a red parallelogram. The zero of energy is set at Fermi level.

C_4N_3 was experimentally realized [29] to possesss an intrinsic half-metallicity for the first time by Du et al. [30] Despite the fact that two-dimensional materials (2DM) hold great potential for a wide range of applications, it will be necessary to modulate their intrinsic properties. Several approaches have been developed to modify the electronic properties of 2DM and hetrostructures. These methods involve substitutional doping, defect engineering, surface functionalization with adatoms, application of an electric field or strain, and by affecting the edge states. Many efforts have been put forth on the electronic properties and modification via this ways. [31–46]

Motivated by the extraordinary properties of these carbon nitrides, we have investigated the structural and electronic properties of van der Waals heterostructures of graphene with C_3N, C_3N_4 and C_4N_3 monolayers by using first-principles calculations. In this work, we have also performed an extensive study of the structural, electronic, and magnetic properties of C_3N, C_3N_4 and C_4N_3, as well as embedded with H, O, S, F, Cl, B, C, N, Si, P, Li, Na, K, Be, Mg, Ca, Al, Sc, Ti, V, Cr, Mn, Fe, Co, Ni and Zn atoms. The embedding of atoms significantly modify the electronic and magnetic properties of pristine C_3N_4 and C_4N_3 nanosheets and the emergence unusual properties such as metallic, half-metallic, spin gapless semiconducting, and dilute-magnetic semiconducting characteristics. Our calculation lead to provide that the band gap and magnetism could be tune by embedding of these atoms. We expect that these interesting phenomena will attract more experimental and theoretical work, and our results also provide significant information about the atom embedding of on C_3N_4 and C_4N_3 nanosheets.

2. Computational Methodology

The first-principle calculations were performed by the OpenMX implemented with the norm-conserving pseudopo-

tentials [47]. The electronic exchange and correlation potential part of the calculations was described by the generalized gradient approximation (GGA) in the Perdew BurkeErnzerhof (GGA-PBE) [48] form applied. The wave functions were expanded into a linear combination of multiple pseudoatomic orbitals (LCPAOs) generated by a confinement scheme [49, 50]. The Brillouin zone (BZ) integration of geometry optimization was represented by a 23×23×1 **k**-point grid in Monkhorst-Pack scheme [51] for the primitive unit cell and scaled according to the size of the supercell. After various convergence tests (as kinetic energy cutoff, k points, etc.), calculations were carried out by using the following parameters: The plane-wave basis set was taken as energy cutoff of 300 Ry; the convergence criterion was taken below 1 meV/Å and 20 Å vacuum spacing along the z-direction to avoid interaction between adjacent layers. The charge transfer was calculated using the Mulliken charge analysis. In order to accurately describe the van der Waals (vdW) interaction, we adopted the empirical correction method presented by Grimme (DFT-D2), [52] which has been proven reliable for describing the long-range vdW interactions.

3. Pristine graphene, C_3N, C_3N_4 and C_4N_3 monolayers

The geometric atomic structures of C_3N, C_3N_4 and C_4N_3 nanosheets are shown in Fig. 1(a-d) (primitive unit cell indicated by a red parallelogram). The graphene crystal has a planar structure with a lattice constant of 2.46 Å and the C-C bond length is 1.42 Å with the C-C-C bond angle being 120°, which is consistent with the value reported by [53–57]. Optimized lattice constant of C_3N is 4.86 Å, while the C-C and C-N bond lengths are 1.404 and 1.403 Å, respectively. The results are in agreement with previous theoretical and experimental results [58–60]. The primitive cell of C_3N_4 involve of three C and four N atoms. The lattice constant of C_3N_4 is determined
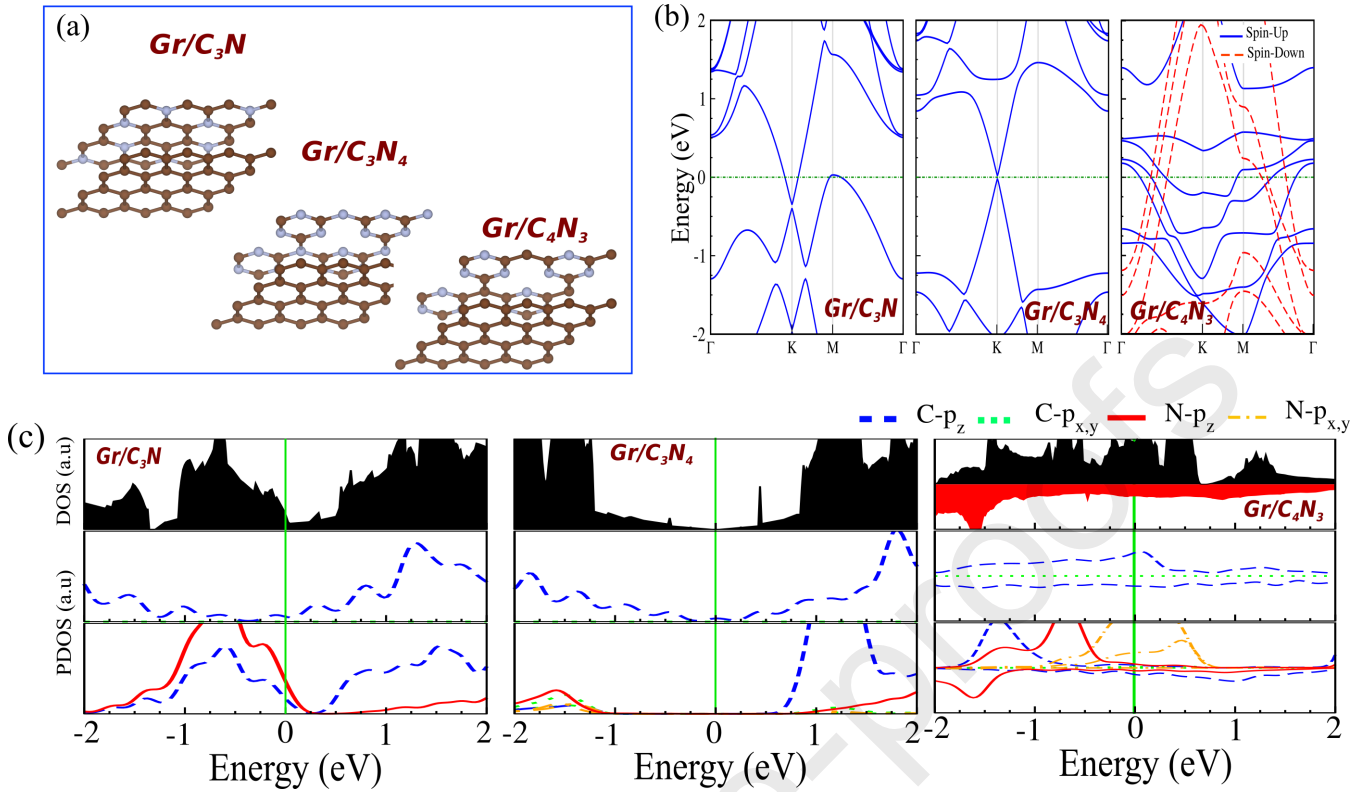
Figure 2: (a) Optimized atomic structures, (b) Electronic structure and (c) DOS and PDOS of graphene/C_3N, graphene/C_3N_4 and graphene/C_4N_3 hetrostructures. With the brown atoms representing C and the blue atoms representing N. The zero of energy is set at Fermi level.

4.74 Å with the N-C-N bond angle being 117.4°, and the two type of bond lengths of C-N is 1.323 and 1.445 Å, respectively. These results are consistent with the previously reported values [61]. After structural relaxation, the calculated lattice constant for C_4N_3 is 4.81 Å, consistent with literature [30, 62–65]. For the most stable structure, the C-C and C-N bond lengths in the ground structure are 1.427 and 1.346 Å, respectively. The difference charge density of graphene, C_3N, C_3N_4 and C_4N_3 are shown in Fig. 1(a-d) in the same panel. The yellow and blue regions represent the charge accumulation and depletion, respectively. We can see a high charge density is found around N atoms in the C_3N, C_3N_4 and C_4N_3. Our result show that each N atom gain about 1.8 electron from the adjacent C atoms in the C_3N. For C_3N_4, each N atom gain about 0.9-2.1 electron from the adjacent C atoms, while N atom gains in the range of 1.2-1.85 electron from the adjacent C atoms in the C_4N_3. The charge redistribution occur in carbon nitride structures due to the different electro-negativities of 2.0 and 3.0 for C and N atoms, respectively.

The electronic structure with corresponding DOS and PDOS of graphene, C_3N, C_3N_4 and C_4N_3, are shown in Fig. 1(b,c). We see that graphene is a semimetal with a zero gap at the E_F, together with the valence and conduction bands crossing with linear dispersion which occur at the K point in the BZ, so-called Dirac-cones. These C-p_z orbitals forms bonding orbital (π) and anti-bonding orbital (π^*) below and above the E_F and touch at one point in the momentum space just at the E_F (see Fig. 1(b)). Our result show that C_3N is a semiconductor with 0.4 eV indi-

rect band gap, while the VBM and CBM are located at Γ and M points (see Fig. 1(b)). Our calculated band gap is in agreement with previous calculations [58, 66, 67]. From PDOS, we see that the VBM of C_3N originated by the N-p_z orbitals and the Dirac-point is formed from N-p_z orbitals, whereas the CBM is prominent by C-p_z orbital states. The C_3N_4 is semiconductor with a direct band gap of 1.45 eV, while the VBM and CBM are located at Γ point (see Fig. 1(b)). This result is in agreement with previous studies [12, 27]. Direct semiconducting behavior of the C_3N_4 can be quite useful for application in nanoelectronics and optoelectronic. For the C_3N_4, the N-s, $p_{x,y}$ orbitals have a significant prominent in the VBM, while N/C-p_z orbitals is prominent in the CBM (see Fig. 1(c)). The C_4N_3 exhibits a half-metal and the degeneracy of up $\uparrow$ and down $\downarrow$ spin channels are broken with 1 μ_B magnetic moment. These results are consistent with previous calculations [30, 63, 65, 68, 69]. For the C_4N_3, the VBM indicates that contributions mainly from the planar C-p_z with N-$p_{x,y}$ orbitals in spin up $\uparrow$ channel and CBM originate from N-$p_{x,y}$ orbitals in spin down $\downarrow$ channel. For the C_4N_3, the half-metallicity and magnetic moment are mainly attributed to the N-$p_{x,y}$ orbitals near the E_F (see Fig. 1(c))

4. Pristine Gr/2D-CN heterostructures

In this section, we have studied electronic properties of vertical heterostructure. 2×2 super cells of graphene and 2D-CN monolayers including of C_3N, C_3N_4 and C_4N_3. The lattice mismatch (δ) between these atomic surfaces is defined as

$\delta = \frac{|a_{up}-a_{dn}|}{a_{dn}} \times 100\%$, where a_{up} and a_{dn} are the lattice constant of upper and down surfaces, respectively. The a_{dn} is taken as increased the twofold of lattice parameter graphene (4.92 Å). The values of lattice constant mismatch between C_3N, C_3N_4, C_4N_3 and graphene are 1.22%, 3.66% and 2.23%, respectively. There is no major distortion in the geometric structures of C_3N, C_3N_4 and C_4N_3 and graphene due to lattice mismatch, and kept that their free-standing states. Four possible configurations of Gr/2D-CN with different stacking patterns were fully relaxed and the interface formation energy was computed by the $E_f = E_{Gr/2D-CN} - E_{Gr} - E_{2D-CN}$, where $E_{Gr/2D-CN}$, E_{Gr} and E_{2D-CN} are the total energies of heterostructure, isolated of Gr and 2D-CN monolayers, respectively. For instance, in the case of Gr/C_3N, we considered four possible stacking, corresponding to the configuration of AA, AB, BA and BB, the formation energies are estimated to be -0.389, -0.394, -0.41 and -0.404 eV, indicating that all the configurations are stable. For the Gr/C_3N, Gr/C_3N_4 and Gr/C_4N_3 hetrostructures the configurations of BA, AB and AB are stable, respectively (Fig. S1). The equilibrium in-terlayer distances are nearly identical in the range of 3.10-3.22Å, indicative of the typical distance of vdW heterostructures. Due to the long-range vdW interaction, the C-C and C-N bond lengths of 1.41Å for Gr/C_3N change very slightly as compared to the freestanding monolayers. To further understand the interaction between Gr and 2D-CN monolayers, the binding energy is defined as $E_b = E_{Gr/2D-CN} - E_{Gr} - E_{2D-CN}$, where $E_{Gr/2D-CN}$, E_{Gr} and E_{2D-CN} are the total energies of heterostructure, isolated of Gr and 2D-CN monolayers, respectively. The binding energies are determined are calculated for Gr/C_3N (19.12 meV/Å^2), Gr/C_3N_4 (17.35 meV/Å^2) and Gr/C_4N_3 (18.41 meV/Å^2), that indicate the weak vdW interaction between the two layers. We can see that the interlayer distance between Gr and 2D-CN monolayers are all in the range of 3.13-3.23 Å, which is a typical vdW equilibrium spacing. These heterostructures have distinctly different values of h, but approximate C-C and C-N bond lengths, which further verifies the weak vdW interactions between the two layers and the chemical bonding force within them. These finding reaffirms Gr/C_3N being an energetically stable vdW heterostructures is in agreement with previous report.[70]

The optimized atomic structures, electronic band structure and DOS of Gr/C_3N, Gr/C_3N_4 and Gr/C_4N_3 are shown in Fig. 2(a-c). The Gr/C_3N, exhibit a metal and in comparison with pristine graphene, the shape of the Dirac-point is changed and shifted to 0.4 eV below of E_F and is located at the K point, similar graphene. It is clearly seen from the DOS and PDOS of Gr/C_3N, that the state at E_F is belong to the N/C-p_z orbital which confirms the metallic behavior (see Fig. 2(c)). Interestingly, Gr/C_3N_4 becomes a semiconductor with narrow band gap of 20 meV, while VBM and CBM are located at K point. Whereas for Gr/C_3N_4 the VBM and CBM are originated from C-p_z and N/C-p_z orbital states, respectively (see Fig. 2(c)). The electronic structure of Gr/C_4N_3 shows a ferromagnetic-metal and the energy bands split into ↑ and ↓ spin channels, resulting in induce 1.3 μ_B magnetic moment. The states around of the E_F in Gr/C_4N_3 mainly originate from of C-p_z and N-$p_{x,y}$ in

the ↑ spin channel, while the degeneracy of ↑ and ↓ spin channels are broken and induce 1.3 μ_B magnetic moment (see Fig. 2(c)). In order to understand that the spin state arrangement on each atom, we have calculated the difference spin density of these heterostructures; blue and red colors show the ↑ and ↓ spin channels, respectively. Our results show that the spin accumulates mainly around N atoms.

5. Effects of different point defects

A schematic model of different type of point defects including typical defects adsorption, site of atom adsorption, insertion and embedding on the heterostructures are shown in Fig. 3(a-c). For obtaining topological defects, we removed C(N) atom from Gr/C_3N to produce single vacancy as called SV_C (SV_N). Double vacancies are created with removing two carbon atoms and one carbon one nitrogen atoms; represented by DV_{CC} and DV_{NC}, respectively. To create the Stone-Wales (SW) defect, we have rotated a single C-C (SW_{CC}) and N-C (SW_{NC}) bond in the C_3N by 90° which labeled as Gr/Defected-C_3N, resulting in a structure with a pair each of respectively, seven-membered and five-membered rings. Adsorption of atom have investigated on the structural, electronic and magnetic properties of pristine C_3N. The most stable sites of various adsorbed atoms are obtained by placing the atom to six stable adsorption
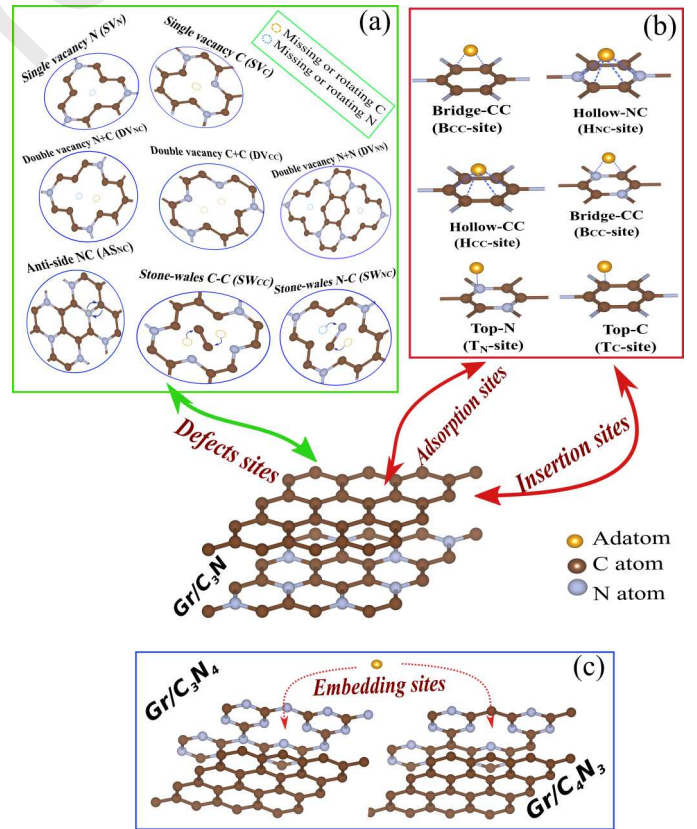

Figure 3: Schematic model of (a) different defects and (b) adsorption and insertion sites of atoms on the graphene/C_3N heterostructure. (c) Schematic model of embedding sites of atoms on the graphene/C_3N_4 and graphene/C_4N_3 heterostructures.
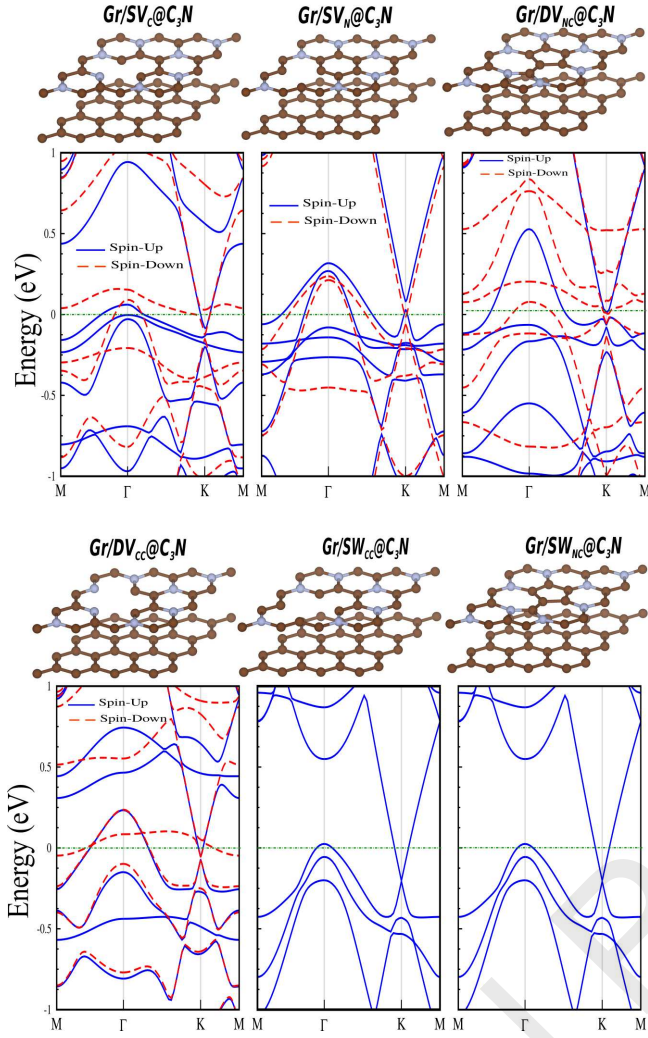
4

Figure 4: Optimized atomic structures and electronic band structures of Gr/C$_3$N with different defects including single, double vacancy, Stone-Wales and anti-site. The zero of energy is set at Fermi level.

sites as schematically illustrated in Fig. 3(b). We have determined the most stable site as the minimum energy configuration among the six different sites where all atoms are relaxed in all directions. These six possible adsorption sites are; (1) the hollow site above the center of a hexagon with six C atoms (H_{CC}), (2) the hollow site above the center of a hexagon composed of both C and N atoms (H_{NC}), (3) the bridge site above the middle of a C-C bond (B_{CC}), (4) the bridge site above the middle of a N-C bond (B_{NC}), (5) the top site above a C atom (T_C), and (6) the top site above a N atom (T_N). In the following adsorbed and inserted Gr/C$_3$N are labeled as Gr/C$_3$N-Adsorbed and Gr/Inserted@C$_3$N, respectively. For instance, H atom adsorbed and inserted Gr/C$_3$N are labeled as Gr/C$_3$N-H and Gr/H@C$_3$N. A schematic view of the atom embedding of site in Gr/C$_3$N$_4$ and Gr/C$_4$N$_3$ is shown in Fig. 3(c). In the following embedded Gr/C$_3$N$_4$ and Gr/C$_4$N$_3$ are labeled as Gr/Embeded-C$_3$N$_4$ and Gr/Embeded-C$_4$N$_3$, respectively.

5.1. Topological defects

Here, we have studied the electronic property of C$_3$N with topological defects on the Gr/Defected@C$_3$N with different defects in Gr/C$_3$N: and in addition vacancies, Stone-Wales and anti-site defects. The fully structural optimization have performed using $2 \times 2 \times 1$ supercell of Gr/C$_3$N which contains 62 atoms (48 C and 16 N atoms). The optimized atomic structures and electronic band structures of Gr/Defected@C$_3$N are shown in Fig. 4. Our result show that the C and N atoms around the vacancy in Gr/C$_3$N undergo a Jahn-Teller distortion [71], and C and N atoms close to the vacancy site move towards each other to form a C-C or C-N bonds. For the reconstructed SV_C and SV_N, two C atoms bond together to build a joint pentagon and nonagon (i.e. the 5-9 configurations). We have observed non-reconstructed structure in the DV_{CC}, whereas DV_{NC} shows a reconstructed structure and two C atoms bond together to build two pentagon and one heptagon (i.e. the 5-8-5 configurations). The distance between dangling bonds in DV_{CC} is found to be 1.404, 1.404 and 1.404 Å (see Fig. 4). After the formation of SW defect, four neighboring hexagons of C$_3$N are transformed into one pentagon and two heptagons (the 55-77 configurations) and C$_3$N maintains its planer structure. The band structure of pristine Gr/C$_3$N is strongly modified by typical defects. Our results demonstrated that the Gr/Defected@C$_3$N with single and double vacancies becomes a ferromagnetic-metal. In addition, the bands split into up ↑ and down ↓ spin channels and induce 1.6 (at SV_C), 1.8 (at SV_N), 2.6 (at DV_{CC}) and 0.7 (DV_{NC}) μ_B magnetic moments in the ground state (see Fig. 4), respectively. While in the Gr/SW@C$_3$N, impurity bands are located in the Fermi level and exhibits a metallic behavior and graphene Dirac-point upon shift to 0.25 below the Fermi level.

5.2. Adsorption and insertion of atoms

The atomic and electronic structure of heterostructures can be controlled by adsorption and insertion inside the interlayer space. To study the effects of adsorption the O, C, Be, Cr, Fe and Co atoms, they placed on intercalate into the interlayer spaces between Gr/C$_3$N are shown in Fig. 5. The impurity bands are located in the Fermi level with a metallic behavior and a band gap opening with value of 50 meV occurs in graphene Dirac-point upon shift to 0.2 eV below the Fermi level for the Gr/C$_3$N-O. Gr/C$_3$N adsorbed with Be, Cr, Fe and Co atoms becomes a ferromagnetic-metal and the bands split into up ↑ and down ↓ spin channels and induce 0.35 , 1.72 , 4.50 , 2.00 and 4.51 μ_B magnetic moments for C, Be, Cr,Fe and C, respectively. The inserted atoms create chemical bonding between the fragments and conduction channels as well as facilitate the carrier transfer between the layers.

The optimized atomic structures and electronic band structures of Gr/C$_3$N inserted with O, C, Be, Cr, Fe and Co atoms are shown in Fig. 5. The Gr/O@C$_3$N, exhibit a semiconductor with negligible band gap of 20 meV that is located at K point. Upon insertion of C, Be, Cr and Fe atoms into Gr/C$_3$N, we have demonstrated that impurity states which are located in around of Fermi level and these systems exhibit a metallic characteristic. The Gr/Co@C$_3$N becomes a ferromagnetic-metal with
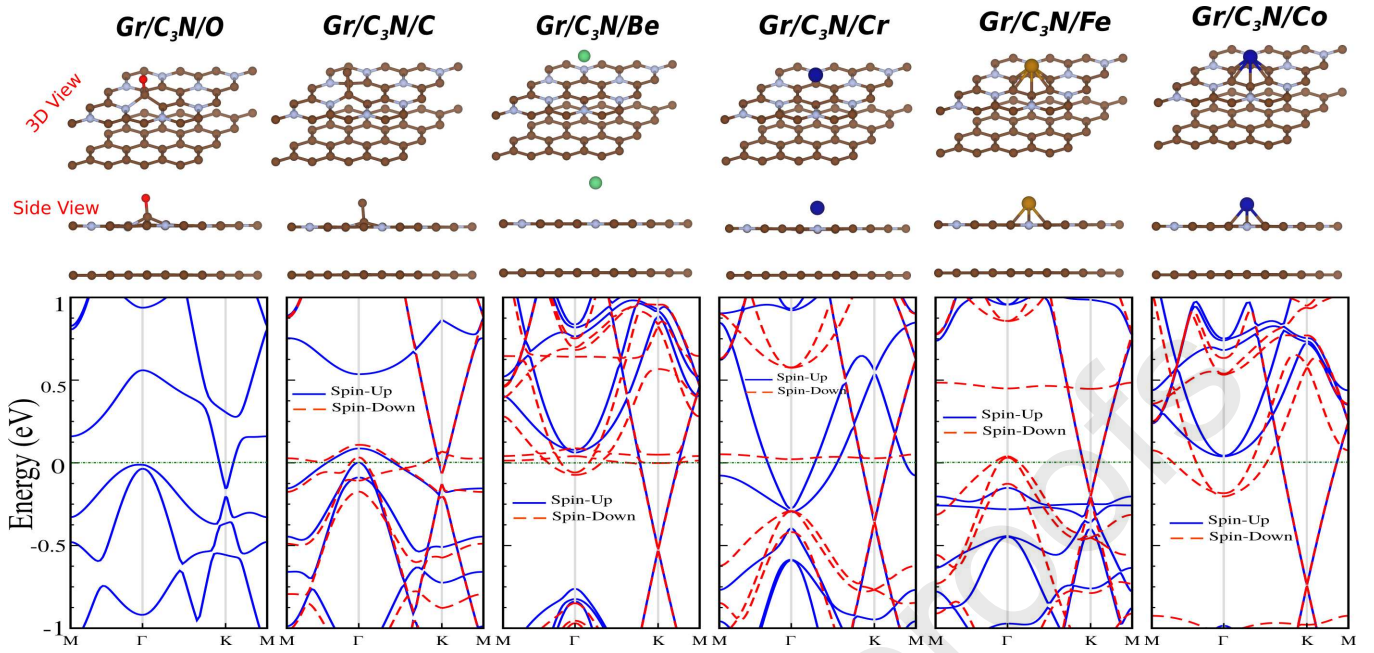
5

Figure 5: Optimized atomic structures and electronic band structures of Gr/C$_3$N adsorbed with O, C, Be, Cr, Fe and Co atoms. The zero of energy is set at Fermi level.
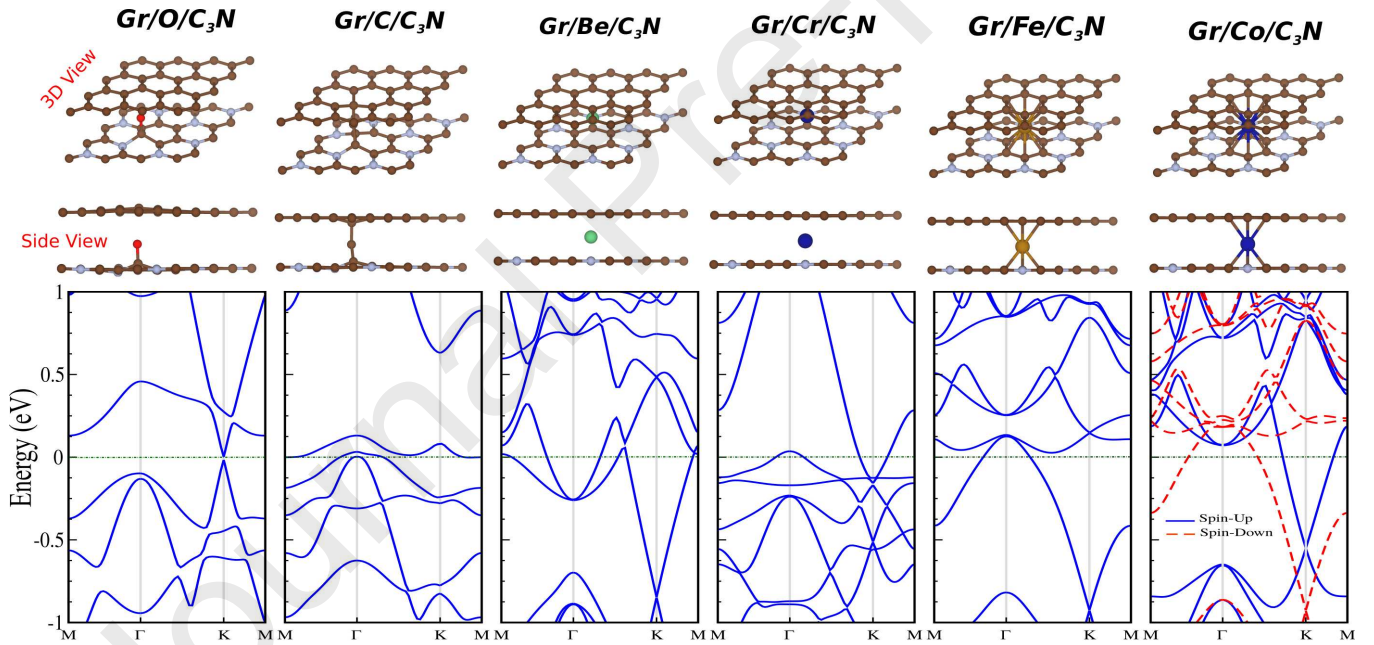

Figure 6: Optimized atomic structures and electronic band structures of Gr/C$_3$N inserted with O, C, Be, Cr, Fe and Co atoms. The zero of energy is set at Fermi level.

1.42 μ_B magnetic moment. The fundamental changes in spin-polarization of graphenes Dirac carriers which caused by adsorption and insertion of atoms on/between the fragments can be used in spin-filtering devices for spintronics applications.

We have explored the geometrical optimization and electronic properties of Gr/C$_3$N$_4$ and Gr/C$_3$N$_4$ heterostructure embedded with H, F, B, Be, Mn and Fe atoms are shown in Fig. 7. The planar lattice of C$_3$N$_4$ and C$_3$N$_4$ is distorted and the honeycomb structures are deformed locally and the host atoms are

pushed away from their equilibrium positions upon the embedding of atoms. The H and F interact through sp^2-hybridization and form one σ bond to neighboring N atoms of Gr/C$_3$N$_4$ and Gr/C$_4$N$_3$, and induces notable structural deformation perpendicular to the surfaces. The bond length of H is 1.34 Å. We see that F is bonded to neighboring N atom in Gr/C$_3$N$_4$ and Gr/C$_4$N$_3$. The F bond length to the nearest N atom is 1.086 Å, and the C-C$_H$-H bond angle is 116°, and there is a distortion out of the plane. The F-C bond lengths are 1.58 and 1.71 Å, while
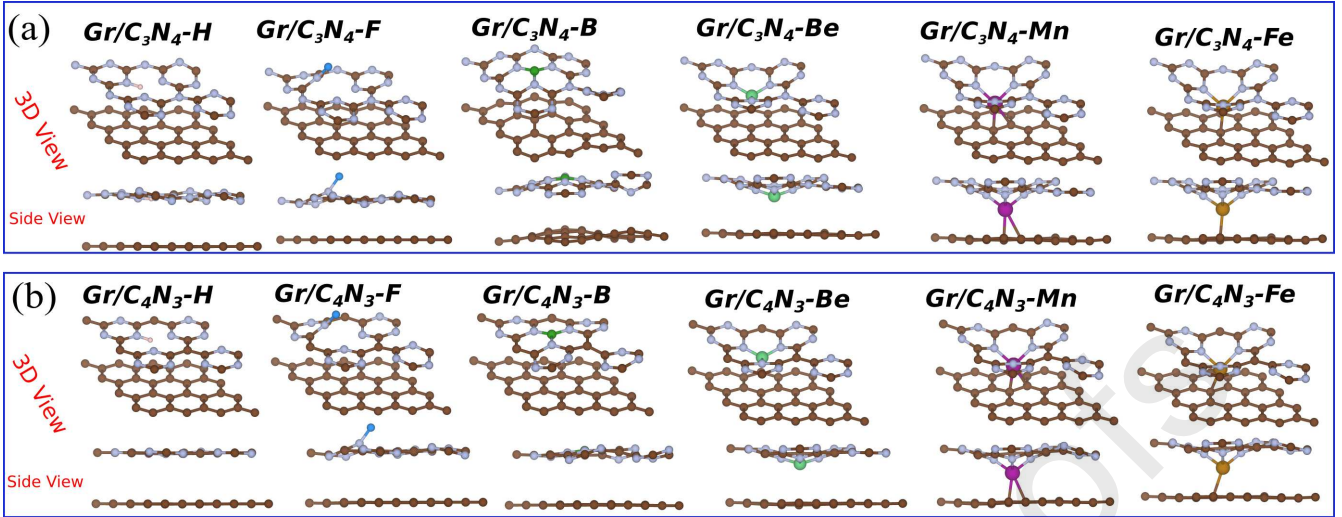
6

Figure 7: Optimized atomic structures and electronic band structures of (a) Gr/C_3N_4 and (b) Gr/C_4N_3 heterostructures embedded with H, F, B, Be, Mn and Fe atoms.
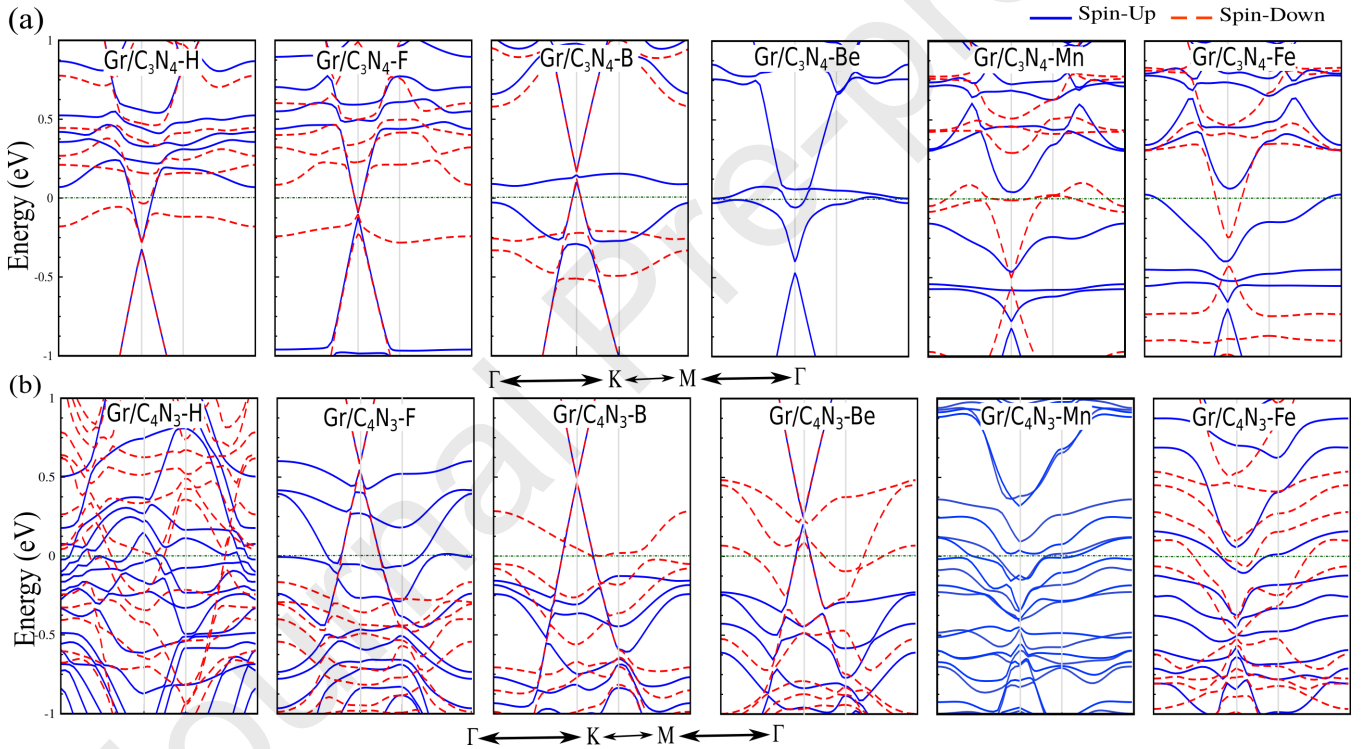
Figure 8: Electronic band structures of (a) Gr/C_3N_4 and (b) Gr/C_4N_3 heterostructures embedded with H, F, B, Be, Mn and Fe atoms. The zero of energy is set at Fermi level.

the C-F-C bond angles are 145 and 119°, suggesting a small effect on the planar structures. Due to the stronger interaction B and Be with Gr/C_3N_4 and Gr/C_4N_3, yield significant distortion, and reconstruction occurs. B and Be interact with through sp^2-hybridization and form three σ bonds with neighboring N atoms. The bond lengths with the nearest N atoms and the C-N-C bond angle are 1.41 Å, 1.42 Å, 119°, respectively. The bond lengths and angles are dependent on the sizes of atoms. Due to changes in the optimized structure, the charge transfer between the atoms and substrate undergo changes as well. The

difference charge densities are presented, where bond formation, charge accumulation, and depletion regions can be clearly seen in the Fig. 3(c,d). The blue and yellow regions represent the charge accumulation and depletion, respectively. It can be seen that electrons are depleted on the atoms of Gr/C_3N_4 and Gr/C_4N_3, whereas the majority of electron enhancement have shown the charge transfer from Gr/C_3N_4 and Gr/C_4N_3 to H and F atoms. These observations indicate a character of covalent bonding and chemisorption.

In order to highlights the underlying mechanism of electronic

7

and magnetic properties, we have considered the spin-polarized band structure. The embedding of atoms gives rise to some localized states in band structure, modifying the electronic properties. The down ↓ spin channel in Mn-C_3N_4 shows a metallic character, while up ↑ spin channels exhibit a semiconductor which implies the half-metallic with 2 μ_B magnetic moment. For the H, F, B and Fe-C_3N_4 is a ferromagnetic metal with the impurity levels crossing E_F with 1, 3, 1 and 2 μ_B magnetic moments, respectively. Our results show that Be-C_3N_4 and Mn-C_4N_3 turns into a metal. Whereas the spin polarization for the H, F, B, Be and Fe-C_4N_3 system in both of the up ↑ and down ↓ spin channels are metal, thus a ferromagnetic-metal can be realized with magnetic moments of 9, 2.7, 1, 2 and 0.5 μ_B, respectively. In comparison with pristine C_3N_4 and C_3N_4, these atoms have been modified to be able to locally change the electronic states and give rise to localized states in the fundamental band gap. The up ↑ spin channel is gap less, while the down ↓ spin channel is semiconducting and the VBM of the ↓ spin channel touches the E_F. The half-metals and spin-glass semiconductors are expected to open up many prospects for practical applications, such as spin photo-diodes, spin detectors, and electromagnetic radiation generators over a various range of wavelengths based on spin photo-conductivity.

6. Conclusion

In summary, extensive DFT-based calculations were carried out to investigate the geometric and electronic properties of graphene/C_3N, C_3N_4 and C_4N_3 van der Waals heterostructure. The C_3N, C_3N_4 with the flat lattices are semiconductors, while the C_4N_3 is a half-metal with significant density of states at Fermi level and 2 μ_B magnetic moment. Our calculations show that vertical heterostructures of graphene on C_3N, C_3N_4 and C_4N_3 exhibits metal, semiconductor (with 20 meV band gap) and ferromagnetic-metal, respectively. The investigation of the effects of various topological defects, such as the single and double vacancies and Stone-Wales defect on the structure and electronic properties of Gr/C_3N are also presented. We found that Gr/C_3N with both single and double vacancies becomes a ferromagnetic-metal. Gr/C_3N becomes an indirect semiconductor with the band gap of 0.2 eV with Stone-Wales defects. Furthermore, we investigated the effects of atoms adsorption and insertion on the electronic property of Gr/C_3N. In the Gr/C_3N-O, impurity bands are located in the Fermi level and exhibits a metallic behavior. Gr/C_3N upon adsorption of Be, Cr, Fe and Co atoms become a ferromagnetic-metal and bands split into up ↑ and down ↓ spin channels and induce 0.35, 1.7, 4.5, 2 and 4.5 μ_B magnetic moments for C, Be, Cr and Fe, respectively. The Gr/C_3N with insertion of O atom exhibits a semiconducting nature with a negligible band gap of 20 meV. Upon the insertion of C, Be, Cr and Fe atoms, band states are excited around the Fermi level and thus these systems exhibit a metallic characteristic. While Co-inserted Gr/C_3N becomes a ferromagnetic-metal with 1.4 μ_B magnetic moment. Finally, we explored the effects of atom embedding on the structural, electronic, and magnetic properties of Gr/C_3N_4 and Gr/C_4N_3. Gr/C_3N_4 with embedding of Mn atom exhibit a half-metal with

2 μ_B magnetic moment, while for the H, F, B and Fe atoms turns into a ferromagnetic metal with 1, 3, 1 and 2 μ_B magnetic moments, respectively. We found that the Gr/C_4N_3 with embedding of Be and Mn turn into a metal, while the spin polarization for the H, F, B, Be and Fe-C_4N_3 system in both of the up ↑ and down ↓ spin channels are metal, thus a ferromagnetic-metal can be realized with magnetic moments of 9, 2.7, 1, 2 and 0.5 μ_B, respectively. Acquires results highlight that the inclusion of typical topological defects, insertion and embedding of atoms in the heterostructures of graphene with carbon nitride nanosheets, can offer appealing ways to further tune the electronic and magnetic properties, and prepare them better for desired applications.

7. Acknowledgment

References

[1] Konstantin S Novoselov, Z Jiang, Y Zhang, SV Morozov, Horst L Stormer, U Zeitler, JC Maan, GS Boebinger, Philip Kim, and Andre K Geim. Room-temperature quantum hall effect in graphene. Science, 315(5817):1379–1379, 2007.

[2] SV Morozov, KS Novoselov, MI Katsnelson, F Schedin, DC Elias, John A Jaszczak, and AK Geim. Giant intrinsic carrier mobilities in graphene and its bilayer. Physical review letters, 100(1):016602, 2008.

[3] Kostya Novoselov. Graphene: Mind the gap. Nature materials, 6(10):720, 2007.

[4] Jonathan da Rocha Martins and Helio Chacham. Disorder and segregation in b- c- n graphene-type layers and nanotubes: tuning the band gap. Acs Nano, 5(1):385–393, 2010.

[5] Yi Ding, Yanli Wang, and Jun Ni. Electronic properties of graphene nanoribbons embedded in boron nitride sheets. Applied Physics Letters, 95(12):123105, 2009.

[6] Natalia Berseneva, Arkady V Krasheninnikov, and Risto M Nieminen. Mechanisms of postsynthesis doping of boron nitride nanostructures with carbon from first-principles simulations. Physical review letters, 107(3):035501, 2011.

[7] O Stephan, PM Ajayan, C Colliex, Ph Redlich, JM Lambert, P Bernier, and P Lefin. Doping graphitic and carbon nanotube structures with boron and nitrogen. Science, 266(5191):1683–1685, 1994.

[8] MO Watanabe, S Itoh, T Sasaki, and K Mizushima. Visible-light-emitting layered b c 2 n semiconductor. Physical review letters, 77(1):187, 1996.

[9] Lijie Ci, Li Song, Chuanhong Jin, Deep Jariwala, Dangxin Wu, Yongjie Li, Anchal Srivastava, ZF Wang, Kevin Storr, Luis Balicas, et al. Atomic layers of hybridized boron nitride and graphene domains. Nature materials, 9(5):430, 2010.

[10] Angel Rubio, Jennifer L Corkill, and Marvin L Cohen. Theory of graphitic boron nitride nanotubes. Physical Review B, 49(7):5081, 1994.

[11] Yandong Ma, Ying Dai, Meng Guo, Chengwang Niu, and Baibiao Huang. Graphene adhesion on mos 2 monolayer: an ab initio study. Nanoscale, 3(9):3883–3887, 2011.

[12] XD Li, S Yu, SQ Wu, YH Wen, S Zhou, and ZZ Zhu. Structural and electronic properties of superlattice composed of graphene and monolayer mos2. The Journal of Physical Chemistry C, 117(29):15347–15353, 2013.

[13] Liam Britnell, RM Ribeiro, A Eckmann, R Jalil, BD Belle, A Mishchenko, Y-J Kim, RV Gorbachev, T Georgiou, SV Morozov, et al. Strong light-matter interactions in heterostructures of atomically thin films. Science, 340(6138):1311–1314, 2013.

[14] He Tian, Zhen Tan, Can Wu, Xiaomu Wang, Mohammad Ali Mohammad, Dan Xie, Yi Yang, Jing Wang, Lain-Jong Li, Jun Xu, et al. Novel field-effect schottky barrier transistors based on graphene-mos 2 heterojunctions. Scientific reports, 4:5951, 2014.

[15] Cory R Dean, Andrea F Young, Inanc Meric, Chris Lee, Lei Wang, Sebastian Sorgenfrei, Kenji Watanabe, Takashi Taniguchi, Phillip Kim, Kenneth L Shepard, et al. Boron nitride substrates for high-quality graphene electronics. Nature nanotechnology, 5(10):722, 2010.

[16] Xiao Lin, Yang Xu, Ayaz Ali Hakro, Tawfique Hasan, Ran Hao, Baile Zhang, and Hongsheng Chen. Ab initio optical study of graphene on hexagonal boron nitride and fluorographene substrates. Journal of Materials Chemistry C, 1(8):1618–1627, 2013.

[17] Jiamin Xue, Javier Sanchez-Yamagishi, Danny Bulmash, Philippe Jacquod, Aparna Deshpande, K Watanabe, T Taniguchi, Pablo Jarillo-Herrero, and Brian J LeRoy. Scanning tunnelling microscopy and spectroscopy of ultra-flat graphene on hexagonal boron nitride. Nature materials, 10(4):282, 2011.

[18] M Neek-Amal, A Sadeghi, GR Berdiyorov, and FM Peeters. Realization of free-standing silicene using bilayer graphene. Applied Physics Letters, 103(26):261904, 2013.

[19] Yongmao Cai, Chih-Piao Chuu, CM Wei, and MY Chou. Stability and electronic properties of two-dimensional silicene and germanene on graphene. Physical Review B, 88(24):245408, 2013.

[20] Wei Hu, Tian Wang, and Jinlong Yang. Tunable schottky contacts in hybrid graphene–phosphorene nanocomposites. Journal of Materials Chemistry C, 3(18):4756–4761, 2015.

[21] Yidong Hou, Anders B Laursen, Jinshui Zhang, Guigang Zhang, Yongsheng Zhu, Xinchen Wang, Søren Dahl, and Ib Chorkendorff. Layered nanojunctions for hydrogen-evolution catalysis. Angewandte Chemie International Edition, 52(13):3621–3625, 2013.

[22] Jiajun Wang, Zhaoyong Guan, Jing Huang, Qunxiang Li, and Jinlong Yang. Enhanced photocatalytic mechanism for the hybrid gc 3 n 4/mos 2 nanocomposite. Journal of Materials Chemistry A, 2(21):7960–7966, 2014.

[23] Nikolaos Tombros, Csaba Jozsa, Mihaita Popinciuc, Harry T Jonkman, and Bart J Van Wees. Electronic spin transport and spin precession in single graphene layers at room temperature. Nature, 448(7153):571, 2007.

[24] Bohayra Mortazavi, Masoud Shahrokhi, Mostafa Raeisi, Xiaoying Zhuang, Luiz Felipe C. Pereira, and Timon Rabczuk. Outstanding strength, optical characteristics and thermal conductivity of graphene-like bc3 and bc6n semiconductors. Carbon, 149:733 – 742, 2019.

[25] Bohayra Mortazavi, Masoud Shahrokhi, Alexander V. Shapeev, Timon Rabczuk, and Xiaoying Zhuang. Prediction of c7n6 and c9n4: stable and strong porous carbon-nitride nanosheets with attractive electronic and optical properties. J. Mater. Chem. C, pages –, 2019.

[26] Javeed Mahmood, Eun Kwang Lee, Minbok Jung, Dongbin Shin, In-Yup Jeon, Sun-Min Jung, Hyun-Jung Choi, Jeong-Min Seo, Seo-Yoon Bae, So-Dam Sohn, et al. Nitrogenated holey two-dimensional structures. Nature communications, 6:6486, 2015.

[27] Guizhi Zhu, Kun Lü, Qiang Sun, Yoshiyuki Kawazoe, and Puru Jena. Lithium-doped triazine-based graphitic c3n4 sheet for hydrogen storage at ambient temperature. Computational Materials Science, 81:275–279, 2014.

[28] Dibyajyoti Ghosh, Ganga Periyasamy, and Swapan K Pati. Transition metal embedded two-dimensional c3n4–graphene nanocomposite: A multifunctional material. The Journal of Physical Chemistry C, 118(28):15487–15494, 2014.

[29] Andrew J Mannix, Brian Kiraly, Mark C Hersam, and Nathan P Guisinger. Synthesis and chemistry of elemental 2d materials. Nature Reviews Chemistry, 1(2):0014, 2017.

[30] Aijun Du, Stefano Sanvito, and Sean C Smith. First-principles prediction of metal-free magnetism and intrinsic half-metallicity in graphitic carbon nitride. Physical review letters, 108(19):197207, 2012.

[31] Asadollah Bafekry, Saber Farjami Shayesteh, and Francois M. Peeters. C₃n monolayer: Exploring the emerging of novel electronic and magnetic properties with adatom adsorption, functionalizations, electric field, charging and strain. J. Phys. Chem. C., 123(19):12485–12499, 2019.

[32] Meysam Bagheri Tagani and Sahar Izadi Vishkayi. Polyaniline (c₃n) nanoribbons: Magnetic metal, semiconductor, and half-metal. J. Appl. Phys., 124(8):084304, 2018.

[33] Thermal conductivity and mechanical properties of nitrogenated holey graphene. Carbon, 106:1 – 8, 2016.

[34] S. Farjami Shayesteh A. Bafekry, M. Ghergherehchi and F.M. Peeters. Adsorption of molecules on c₃n nanosheet: A first-principles calculations. Chem. Phys., 526:110442, 2019.

[35] M. Yagmurcukardes. Monolayer fluoro-inse: Formation of a thin monolayer via fluorination of inse. Phys. Rev. B, 100:024108, Jul 2019.

[36] Asadollah Bafekry, Mitra Ghergherehchi, and Saber Farjami Shayesteh. Tuning the electronic and magnetic properties of antimonene nanosheets via point defects and external fields: first-principles calculations. Phys. Chem. Chem. Phys., 21:10552–10566, 2019.

[37] Berna Akgenc. Intriguing of two-dimensional janus surface-functionalized mxenes: An ab initio calculation. Computational Materials Science, 171:109231, 2020.

[38] A. Bafekry, B. Mortazavi, and S. Farjami Shayesteh. Band gap and magnetism engineering in dirac half-metallic na2c nanosheet via layer thickness, strain and point defects. Journal of Magnetism and Magnetic Materials, 491:165565, 2019.

[39] Khang D. Pham, Nguyen N. Hieu, Huynh V. Phuc, I. A. Fedorov, C. A. Duque, B. Amin, and Chuong V. Nguyen. Layered graphene/gas van der waals heterostructure: Controlling the electronic properties and schottky barrier by vertical strain. Applied Physics Letters, 113(17):171605, 2018.

[40] A. Bafekry, C. Stampfl, S. Farjami Shayesteh, and F. M. Peeters. Exploiting the novel electronic and magnetic structure of c3n via functionalization and conformation. Advanced Electronic Materials, 0(0):1900459.

[41] B. Akgenc. Two-dimensional black arsenic for li-ion battery applications: a dft study. Journal of Materials Science, 54(13):9543–9552, Jul 2019.

[42] Khang D. Pham, Nguyen N. Hieu, Huynh V. Phuc, Bui D. Hoi, Victor V. Ilysov, Bin Amin, and Chuong V. Nguyen. First principles study of the electronic properties and schottky barrier in vertically stacked graphene on the janus moses under electric field. Computational Materials Science, 153:438 – 444, 2018.

[43] Asadollah Bafekry, Saber Farjami Shayesteh, and Francois M. Peeters. Introducing novel electronic and magnetic properties in c3n nanosheets by defect engineering and atom substitution. Phys. Chem. Chem. Phys., 21:21070–21083, 2019.

[44] P.T.T. Le, Le M. Bui, Nguyen N. Hieu, Huynh V. Phuc, B. Amin, Nguyen V. Hieu, and Chuong V. Nguyen. Tailoring electronic properties and schottky barrier in sandwich heterostructure based on graphene and tungsten diselenide. Diamond and Related Materials, 94:129 – 136, 2019.

[45] M. Ghergherehchi A. Bafekry, S. F. Shayesteh and F. M. Peeters. Tuning the band gap and introducing magnetism into monolayer bc₃ by strain/defect engineering and adatom/molecule adsorption. J. Appl. Phys., 2019.

[46] H. U. Din, M. Idrees, Gul Rehman, Chuong V. Nguyen, Li-Yong Gan, Iftikhar Ahmad, M. Maqbool, and B. Amin. Electronic structure, optical and photocatalytic performance of sicmx2 (m = mo, w and x = s, se) van der waals heterostructures. Phys. Chem. Chem. Phys., 20:24168–24175, 2018.

[47] Norman Troullier and José Luís Martins. Efficient pseudopotentials for plane-wave calculations. Physical review B, 43(3):1993, 1991.

[48] John P Perdew, Kieron Burke, and Matthias Ernzerhof. Generalized gradient approximation made simple. Physical review letters, 77(18):3865, 1996.

[49] Taisuke Ozaki. Variationally optimized atomic orbitals for large-scale electronic structures. Physical Review B, 67(15):155108, 2003.

[50] T Ozaki and H Kino. Numerical atomic basis orbitals from h to kr. Physical Review B, 69(19):195113, 2004.

[51] Hendrik J Monkhorst and James D Pack. Special points for brillouin-zone integrations. Physical review B, 13(12):5188, 1976.

[52] Tomas Bucko, Jurgen Hafner, Sébastien Lebegue, and János G Angyán. Improved description of the structure of molecular and layered crystals: ab initio dft calculations with van der waals corrections. The Journal of Physical Chemistry A, 114(43):11814–11824, 2010.

[53] AH Castro Neto, Francisco Guinea, Nuno MR Peres, Kostya S Novoselov, and Andre K Geim. The electronic properties of graphene. Reviews of modern physics, 81(1):109, 2009.

[54] Kostya S Novoselov, D Jiang, F Schedin, TJ Booth, VV Khotkevich, SV Morozov, and Andre K Geim. Two-dimensional atomic crystals. Proceedings of the National Academy of Sciences, 102(30):10451–10453, 2005.

[55] Yafei Li, Zhen Zhou, Guangtao Yu, Wei Chen, and Zhongfang Chen. Co catalytic oxidation on iron-embedded graphene: computational quest for low-cost nanocatalysts. The Journal of Physical Chemistry C, 114(14):6250–6254, 2010.

[56] Alexander A Balandin, Suchismita Ghosh, Wenzhong Bao, Irene Calizo, Desalegne Teweldebrhan, Feng Miao, and Chun Ning Lau. Superior thermal conductivity of single-layer graphene. Nano letters, 8(3):902–907, 2008.

[57] Andre K Geim and Konstantin S Novoselov. The rise of graphene. In Nanoscience and Technology: A Collection of Reviews from Nature Journals, pages 11–19. World Scientific, 2010.

[58] Javeed Mahmood, Eun Kwang Lee, Minbok Jung, Dongbin Shin, Hyun-Jung Choi, Jeong-Min Seo, Sun-Min Jung, Dongwook Kim, Feng Li, Myoung Soo Lah, et al. Two-dimensional polyaniline (c3n) from carbonized organic single crystals in solid state. Proceedings of the National Academy of Sciences, 113(27):7414–7419, 2016.

[59] Seiji Mizuno, Mitsutaka Fujita, and Kenji Nakao. Electronic states of graphitic heterocompounds of carbon, boron and nitrogen. Synthetic Metals, 71(1-3):1869–1870, 1995.

[60] Bohayra Mortazavi. Ultra high stiffness and thermal conductivity of graphene like c_3n. Carbon, $118:25--34, 2017$.

[61] Edwin Kroke, Marcus Schwarz, Elisabeth Horath-Bordon, Peter Kroll, Bruce Noll, and Arlan D Norman. Tri-s-triazine derivatives. part i. from trichloro-tri-s-triazine to graphitic c 3 n 4 structures. New Journal of Chemistry, 26(5):508–512, 2002.

[62] Arqum Hashmi, M Umar Farooq, Tao Hu, and Jisang Hong. Spin-dependent transport and optical properties of transparent half-metallic g-c4n3 films. The Journal of Physical Chemistry C, 119(4):1859–1866, 2015.

[63] Arqum Hashmi and Jisang Hong. Metal free half metallicity in 2d system: structural and magnetic properties of gc 4 n 3 on bn. Scientific reports, 4:4374, 2014.

[64] Chung-Huai Chang, Xiaofeng Fan, Shi-Hsin Lin, and Jer-Lai Kuo. Orbital analysis of electronic structure and phonon dispersion in mos 2, mose 2, ws 2, and wse 2 monolayers under strain. Physical Review B, 88(19):195420, 2013.

[65] Xiaoming Zhang, Mingwen Zhao, Aizhu Wang, Xiaopeng Wang, and Aijun Du. Spin-polarization and ferromagnetism of graphitic carbon nitride materials. Journal of Materials Chemistry C, 1(39):6265–6270, 2013.

[66] Qianku Hu, Qinghua Wu, Haiyan Wang, Julong He, and Guanglei Zhang. First-principles studies of structural and electronic properties of layered c3n phases. physica status solidi (b), 249(4):784–788, 2012.

[67] HJ Xiang, Bing Huang, ZY Li, S-H Wei, JL Yang, and XG Gong. Ordered semiconducting nitrogen-graphene alloys. Physical Review X, 2(1):011003, 2012.

[68] Tao Hu, Arqum Hashmi, and Jisang Hong. Transparent half metallic gc 4 n 3 nanotubes: potential multifunctional applications for spintronics and optical devices. Scientific reports, 4:6059, 2014.

[69] Haiping Wu, Yuzhen Liu, Erjun Kan, Yanming Ma, Wenjie Xu, Jie Li, Meichen Yan, Ruifeng Lu, Jianfeng Wei, and Yan Qian. The diverse electronic properties of c4n3 monolayer under biaxial compressive strain: a theoretical study. Journal of Physics D: Applied Physics, 49(29):295301, 2016.

[70] Yiran Wang, Zhaoyong Jiao, Shuhong Ma, and Yongliang Guo. Probing c3n/graphene heterostructures as anode materials for li-ion batteries. Journal of Power Sources, 413:117 – 124, 2019.

[71] Hermann Arthur Jahn and Edward Teller. Stability of polyatomic molecules in degenerate electronic states-iorbital degeneracy. Proceedings of the Royal Society of London. Series A-Mathematical and Physical Sciences, 161(905):220–235, 1937.

- Electronic and magnetic properties of graphene/carbon-nitride heterostructures are studied.
- Effects of embedding of various atoms and defects on resulting properties are explored.
- Electronic nature and magnetism can be effectively modified in the considered heterostructures.